

## Study of the low-frequency Raman scattering in $\text{NaNbO}_3$ crystal

This article has been downloaded from IOPscience. Please scroll down to see the full text article.

2003 J. Phys.: Condens. Matter 15 1387

(<http://iopscience.iop.org/0953-8984/15/9/302>)

View [the table of contents for this issue](#), or go to the [journal homepage](#) for more

Download details:

IP Address: 171.66.16.119

The article was downloaded on 19/05/2010 at 06:38

Please note that [terms and conditions apply](#).

# Study of the low-frequency Raman scattering in $\text{NaNbO}_3$ crystal

E Bouziane<sup>1,2</sup>, M D Fontana<sup>1,3</sup> and M Ayadi<sup>2</sup>

<sup>1</sup> Laboratoire Matériaux Optiques, Photonique et Systèmes, FRE CNRS 2304, Université de Metz et Supélec, 2 Rue E Belin, 57070 Metz Cedex, France

<sup>2</sup> Laboratoire de Physique des Matériaux et d'Electronique, Faculté des Sciences I, Aïn Chock, Université Hassan II, Casablanca, Morocco

Received 19 June 2001, in final form 30 January 2003

Published 24 February 2003

Online at [stacks.iop.org/JPhysCM/15/1387](http://stacks.iop.org/JPhysCM/15/1387)

## Abstract

The Raman scattering spectrum of the sodium niobate crystal, in both P and R phases, has been investigated from room temperature up to 440 °C. The dependence of the low-frequency (LF) spectrum clearly reveals, for the first time, over a wide temperature range, the presence of a strong quasi-elastic scattering below a LF zone centre phonon. The phase transition mechanism is discussed, considering an order–disorder process induced by the relaxation of the Nb ions.

## 1. Introduction

Sodium niobate  $\text{NaNbO}_3$  exhibits a very complex sequence of structural phase transitions with changing temperature. The structure and the symmetry of each phase were determined by means of x-ray diffraction measurements [1, 2].

$\text{NaNbO}_3$  has the prototype cubic phase above 641 °C and then undergoes transformations at 640, 575, 520, 480 and 370 °C. The successive phases, which are labelled  $T_2$ ,  $T_1$ , S, R and P, are of orthorhombic symmetry except  $T_2$  which is tetragonal. At low temperature a phase N with rhombohedral symmetry occurs below –80 °C [3]. The structures and symmetries of several phases are still controversial. Using high-resolution neutron scattering, Darlington and Knight [3] have recently shown that the symmetry of the room temperature (RT) phase P should be monoclinic rather than orthorhombic.

An additional phase transition at 190 °C was recently proposed [4], whereas new phases can be induced by doping or applying an electric field [1, 5–7]. All phase transitions are antiferrodistortive and associated with a tilt of the  $\text{NbO}_6$  octahedron.

It was shown by means of dielectric measurements that the phases P and R are antiferroelectric (AFE) whereas the low-temperature phase N is ferroelectric [8].

<sup>3</sup> Author to whom any correspondence should be addressed.

Just a few investigations dealt with the mechanism of the phase transitions, by means of infrared and Raman spectroscopy. Raman spectra of powder samples have been studied from RT up to 480 °C [4] as well as at low temperature down to 10 K [9]. The behaviours of the Raman bands were analysed with temperature change but these results did not provide any information about the process inducing the structural phase transitions.

Here we present new Raman scattering measurements which, for the first time, were recorded for single crystals, allowing a study for various light polarizations. Special attention was devoted to the behaviour of the low-frequency (LF) spectrum.

## 2. Experimental results

### 2.1. Experimental conditions

Raman measurements were carried out in right-angle scattering geometries on a parallelepiped  $\text{NaNbO}_3$  single crystal. Spectra were obtained with a Spex double monochromator, model 1401, using a photon-counting system and linked with a Datamate micro-processor spectrometer controller and data acquisition processor. The Spectra Physics helium–neon laser line of 6328 Å wavelength and 50 mW power was used. All Raman spectra were recorded in the same experimental conditions within a resolution of  $0.2 \text{ cm}^{-1}$  using narrow slits. For the measurements between RT and 440 °C the sample was mounted in a temperature-controlled furnace. The spectra were recorded several times in the same conditions and data were accumulated in order to detect less intense lines and to improve the signal-to-noise ratio. The propagation directions of the incident and scattered light were generally along the  $Y$ - and  $X$ -axes, respectively (where the  $X$ -,  $Y$ -,  $Z$ -axes are the crystallographic axes).

The spectra were measured on heating, under the same experimental conditions, in  $Y(ZZ)X$  and  $Y(ZY)X$  configurations, where the letters in brackets denote the polarizations of the incident and scattered light, in that order.

### 2.2. Raman spectra at room temperature

At RT, according to the orthorhombic structure (point group  $D_{2h}^{11}$ ) corresponding to eight molecular units per unit cell, the irreducible representations of the optical vibrational modes at zero wavevector are

$$\Gamma = 15A_g + 17B_{1g} + 15B_{2g} + 13B_{3g} + 13A_u + 14B_{1u} + 16B_{2u} + 14B_{3u}$$

where the  $A_g$ ,  $B_{1g}$ ,  $B_{2g}$  and  $B_{3g}$  modes are only Raman active, whereas the  $A_u$  modes are inactive and the  $B_{1u}$ ,  $B_{2u}$  and  $B_{3u}$  modes are infrared active.

60 optically Raman-active phonons are expected; however, only 20 Raman lines were clearly detected in the spectrum recorded at RT. This is probably due to the intensity of some lines being very weak, while other lines are hidden by more intense peaks lying in the neighbourhood. The Raman spectrum recorded at RT in the  $(ZZ)$  configuration is reported in figure 1. This spectrum was found to be independent of the polarization of the incident and scattered light. Indeed the same features were observed in all configurations. This indicates that the crystal probably has a polydomain character in the antiferroelectric P phase.

As usual for the oxide perovskites, three frequency ranges can be distinguished: the LF range ( $\omega \leq 200 \text{ cm}^{-1}$ ), the intermediate-frequency (IF) range ( $200\text{--}450 \text{ cm}^{-1}$ ) and the high-frequency (HF) range ( $450\text{--}800 \text{ cm}^{-1}$ ). The LF range displays eight structures labelled 1–8. The two strongest peaks, Nos 1 and 2, are located at 64 and 74  $\text{cm}^{-1}$ . Several peaks (Nos 10, 13, 14, 16, 17) and shoulders in these peaks ( $S_9$ ,  $S_{11}$ ,  $S_{12}$ ,  $S_{15}$ ) are observed in the IF range.

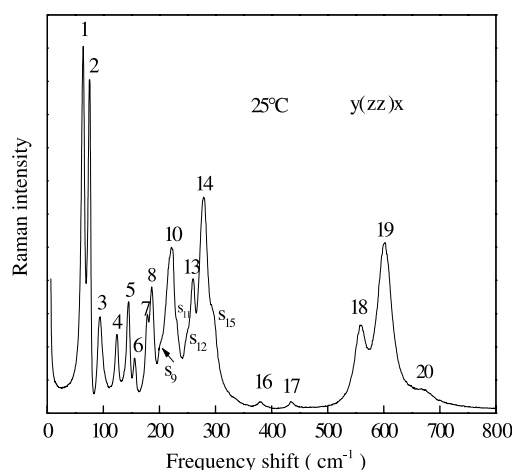


**Figure 1.** Raman spectra recorded for  $\text{NaNbO}_3$  at RT in the configuration  $Y(ZZ)X$ .

Three peaks (Nos 18–20) are depicted above  $500\text{ cm}^{-1}$  and, like for other oxide perovskites, can be attributed to oxygen ion motions.

### 2.3. Temperature dependence of the Raman spectra

Figure 2 shows typical Raman spectra recorded in the  $(ZZ)$  configuration for various temperatures over the whole frequency range. On heating from RT up to  $380^\circ\text{C}$ , the spectrum shows changes in lineshape, maximum location and intensity of the peaks, especially below  $100\text{ cm}^{-1}$ , but also in the ranges  $150\text{--}300$  and  $500\text{--}650\text{ cm}^{-1}$ . Increasing temperature is accompanied by several features:

- (1) All lines become broader.
- (2) Several peaks in the IF range ( $100\text{--}300\text{ cm}^{-1}$ ) coalesce to give rise to a more complicated lineshape (see the spectra recorded at  $140$  and  $190^\circ\text{C}$ ). It is however remarkable that above  $190^\circ\text{C}$  some lines are again clearly distinct, despite their broadening.
- (3) The high-energy lines 18 and 19 above  $500\text{ cm}^{-1}$  coalesce into a large broad band which decreases in frequency and is still present in the phase R.
- (4) The peaks  $S_{15}$ , 16, 17 and 20 disappear with increasing temperature.

The largest change with temperature occurs in the LF range of the spectrum. First, the double-peaked structure corresponding to the lowest-frequency lines 1 and 2 detected at RT is still discernible but less and less resolved upon heating, from RT to  $190^\circ\text{C}$ , and shifts down in frequency. Above  $240^\circ\text{C}$ , only an asymmetric line attributed to the low-frequency mode (LFM), which results from the superposition of lines 1 and 2, is detected (figures 2(b) and (c)). Dramatic spectral changes are observed (see figure 2(c)) at the P–R phase transition, which takes place between  $370$  and  $380^\circ\text{C}$ , according to [1]. Above this transition temperature, the spectrum in the AFE phase R shows only four peaks: a highly damped LF peak and three broad bands denoted as A, B and C.

### 2.4. Low-frequency spectra

To give a careful description of the behaviour of the features at LF in both P and R phases and through the P–R phase transition, we report in figure 3 the LF spectrum as a function of

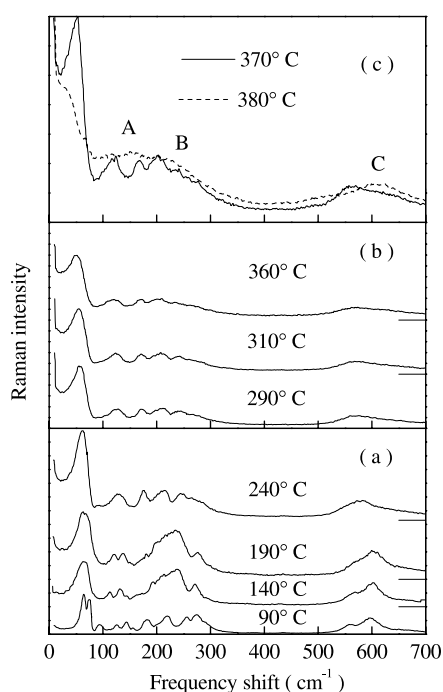


**Figure 2.** Complete Raman spectra recorded for  $\text{NaNbO}_3$  in the configuration (ZZ) at various temperatures. All spectra are reported on the same scale. The baseline for each spectrum is indicated by the horizontal line.

temperature recorded in the (ZZ) configuration. A quasi-elastic scattered signal (QES) appears below the LF peak, for temperatures above  $240^\circ\text{C}$ . This QES is revealed by the change in the lineshape and the slope of the LF scattering below  $25\text{ cm}^{-1}$ . The apparent asymmetry of the LFM is partly due to the overlapping with the QES. It can be mentioned that no QES was reported in the previous Raman investigation [4].

In phase P, the intensity of the LFM increases and its maximum seems to shift down towards the QES. Above  $370^\circ\text{C}$  in the vicinity of the P–R phase transition (figure 3(b)), the LFM decreases in both frequency and intensity whereas its linewidth increases. Above  $380^\circ\text{C}$  (figure 3(c)) in the R phase, the LF Raman profile still contains a QES and this situation holds on heating up to  $440^\circ\text{C}$ .

In order to get information about the origin of the QES, we also compare in figure 3 the LF spectra recorded in two different configurations, (ZZ) and (ZY), for several temperatures. It should be mentioned that no polarized Raman scattering in  $\text{NaNbO}_3$  has been reported previously.

Below  $370^\circ\text{C}$  in the P phase, the spectra recorded in the two configurations exhibit exactly the same features. In contrast, through and above the P–R phase transition the LF spectrum was found to be sensitive to the polarization of the scattered light. Thus the (ZZ) spectrum consists of a central component with a broad shoulder whereas the (ZY) profile contains only a wide band centred on zero, as shown in figure 4. The LF (ZY) profile does not exhibit any change in shape for all temperatures above the phase transition and only the intensity level depends on the temperature. This spectrum can be fitted to damped oscillators, whose frequencies are close, giving rise to a flat and broad scattered intensity. (see figure 4(b)). This feature can be interpreted as the disappearance of the QES in the (ZY) geometry through the P–R transition.

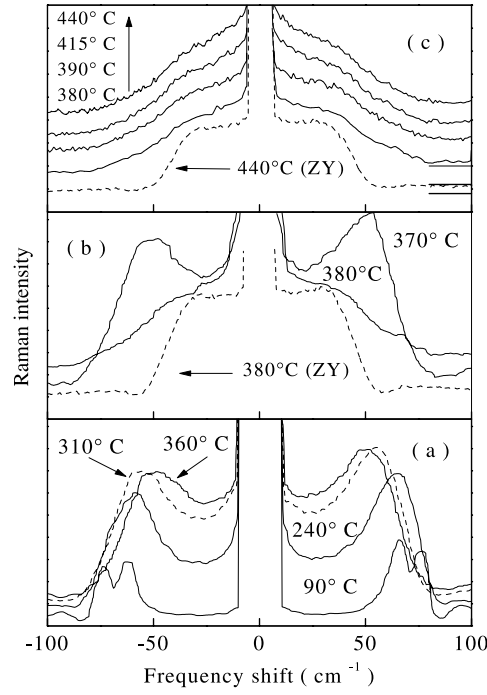


**Figure 3.** LF Raman spectra recorded for NaNbO<sub>3</sub> in the configuration (ZZ) at various temperatures. For comparison we also report spectra recorded in the configuration (ZY) at 380 and 440 °C.

### 3. Analysis of Raman results

Now we analyse the LF (ZZ) Raman data as a function of the temperature and their possible relation with the P–R phase transition. For this, we assume that the QES arises from a Debye relaxation mode and that it does not interact with the LFM. Thus, we fit the Raman spectra to a sum of relaxator and damped harmonic oscillators:

$$I_R(\omega) = \frac{I(\omega)}{\omega[n(\omega) + 1]} = \sum_j K_j \frac{\omega_j^2 \Gamma_j}{(\omega_j^2 - \omega^2)^2 + \omega^2 \Gamma_j^2} + K' \frac{\gamma_r}{\omega^2 + \gamma_r^2} \quad (1)$$

where  $I(\omega)$  denotes the experimental scattered intensity,  $n(\omega) + 1$  is the Bose–Einstein population factor for the Stokes scattering,  $\omega_j$  and  $\Gamma_j$  are the frequency and damping of the  $j$ th phonon,  $\gamma_j$  is the inverse relaxation time,  $K_j$  and  $K'$  are the intensity factors for the oscillator  $j$  and the relaxator strength respectively. Some examples of the fit are reported in figure 5. The good agreement which was achieved between the calculated and experimental spectra is illustrated for several temperatures.

First we discuss the temperature dependence of the intensity of the LF features, i.e. the QES and the LFM. Instead of the factors  $K$  and  $K'$  we consider the renormalized integrated intensity of the QES and the LFM peaks, as calculated from

$$J = \int_a^b \frac{I(\omega)}{\omega(n(\omega) + 1)} d\omega \quad (2)$$

where  $a$  and  $b$  correspond to the LF and HF limits of the peak. As shown in figure 6(a), the integrated intensities of the two features exhibit similar behaviours versus temperature.

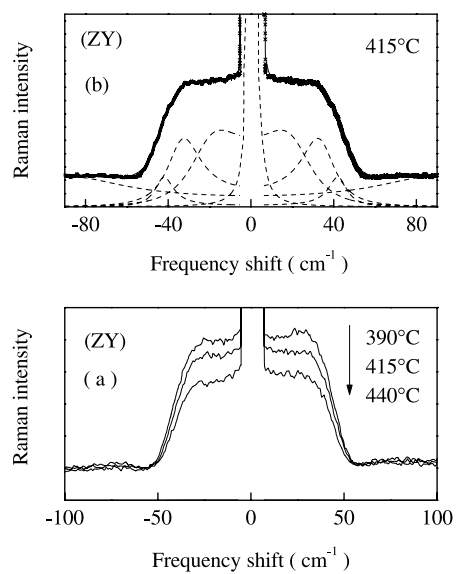


**Figure 4.** (a) LF Raman spectra recorded for NaNbO<sub>3</sub> in the configuration (ZY) at various temperatures. (b) The Raman spectrum recorded at 415 °C fitted to a Lorentzian peak (Rayleigh line) and four damped harmonic oscillators. Experimental data are represented by symbols and calculated results by the dashed curves.

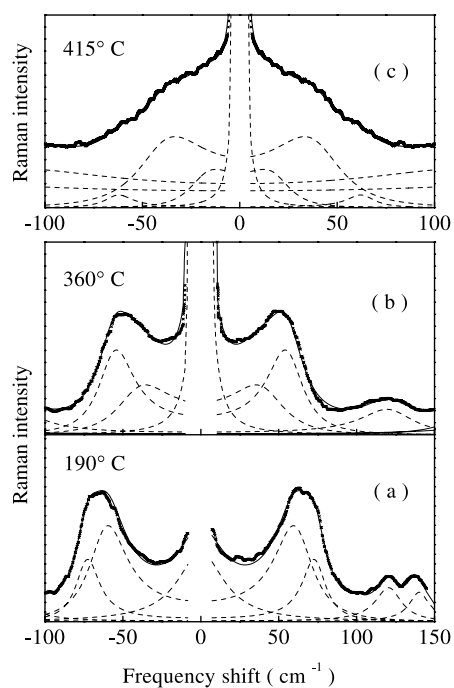


**Figure 5.** Typical (ZZ) Raman spectra fitted to equation (1). Experimental data are represented by symbols. The dashed curves are calculated spectra. The dash-dot curves in part (c) correspond to the contribution of the bands A and B illustrated in figure 2(c).

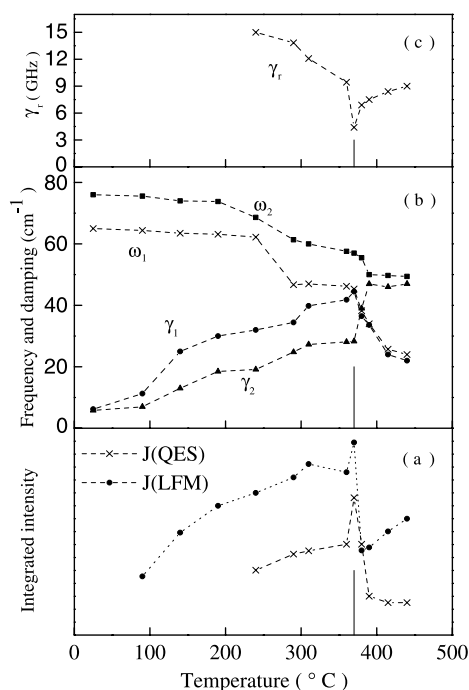


**Figure 6.** Temperature dependences of the fit parameters. (a) Integrated intensities of the QES  $J$  and the LFM  $J$ . (b) The frequency and damping of the LFM. (c) The inverse of the relaxation time of the central peak in  $\text{NaNbO}_3$ . The temperature  $T_{tr}$  is denoted by the vertical solid line.

This proves that no intensity transfer occurs between the QES and LFM, and thus justifies the assumption of no coupling in equation (1).

The maxima of intensity in  $J(\text{QES})$  and  $J(\text{LFM})$  are close to each other and correspond to the phase transition temperature  $T_{tr} = 370^\circ\text{C}$ , in good agreement with previous dielectric data [10].

The integrated intensity of the LFM  $J$  (figure 6(a)) strongly increases on heating from RT up to  $310^\circ\text{C}$ , then shows a plateau and a small increase on approaching  $T_{tr}$ . Above the P–R phase transition the integrated intensity of the LFM abruptly decreases and, finally, increases again when heated above  $380^\circ\text{C}$  in the R phase. In P phase and far from  $T_{tr}$  ( $370^\circ\text{C}$ ), the QES integrated intensity  $J(\text{QES})$  increases slightly from  $240$  up to  $360^\circ\text{C}$ , then more strongly on approaching the P–R phase transition. Above the phase transition,  $J(\text{QES})$  decreases but the QES still exists in the R phase and its integrated intensity is found to be nearly constant for temperatures above  $390^\circ\text{C}$ .

Now we discuss the frequency and damping of the LFM (peaks 1 and 2) as derived from fit calculations. As shown in figure 6(b), the frequencies of the phonons 1 and 2 continuously decrease and their dampings increase with increasing temperature on approaching the phase transition. It should be mentioned that the frequency strongly differs from the position of the peak maximum owing to the phonon damping. This damping is very large above  $200^\circ\text{C}$ , especially for phonon 1. Thus at  $360^\circ\text{C}$ , a fit of the  $ZZ$  spectrum yields for the lowest phonon (phonon 1) a value of the frequency of  $46\text{ cm}^{-1}$  (damping  $42\text{ cm}^{-1}$ ), whereas the peak maximum position lies around  $35.5\text{ cm}^{-1}$ . Phonon 2 is less affected by its damping ( $28\text{ cm}^{-1}$ ) at this temperature, so the calculated frequency ( $58\text{ cm}^{-1}$ ) is close to the peak maximum position ( $54\text{ cm}^{-1}$ ).



Above the transition temperature  $T_{tr}$ , both the frequency and the damping of peak 1 as well as the frequency of mode 2 decrease with increasing temperature, then become nearly constant in phase R.

The dependence of the inverse of the relaxation time of the central peak is plotted in figure 6(c).  $\gamma_r$  decreases on heating from 240 °C up to  $T_{tr}$  and increases in the R phase. Since it decreases on approaching  $T_{tr}$  from above and below,  $\gamma_r$  displays a critical slowing down which is connected with the phase transition.

#### 4. Discussion

In the light of our results obtained on the sodium niobate crystal, we suggest the nature and a transition mechanism of the P–R phase transition. For this, we consider, as the main experimental feature in the Raman spectra, the existence of an anisotropic QES besides a slight softening of the LF phonons.

We point out that the phonon lines 1 and 2 at the zone centre modes arise from zone boundary phonons associated with rotation of the  $\text{NbO}_6$  octahedra and therefore are related to the antiferrodistortive nature of the transition, which leads to a folding of the Brillouin zone.

As emphasized above, the QES exists in the (ZZ) geometry over a large temperature range and around  $T_{tr}$ , but only below  $T_{tr}$  in the (ZY) configuration. The occurrence of the QES in both phases P and R reveals the existence of polar clusters in the AFE states.

Such a central peak was earlier detected in other niobates such as  $\text{KNbO}_3$  [11], KTN [12] and  $\text{LiNbO}_3$  [13]. Therefore it can be attributed to a relaxation process of off-centre Nb ions between two equivalent positions within the oxygen octahedra. The off-centring displacements of Nb ions are responsible for a disorder in the lattice but yield a zero average polarization. A similar disorder phenomenon was reported in other AFE materials such as  $\text{PbZrO}_3$  [14] and  $\text{AgNbO}_3$  [15]. The presence below  $T_{tr}$  of the QES in both (ZZ) and (ZY) spectra indicates the existence of several clusters randomly distributed with different sizes and polarizations. The anisotropy of the QES in the phase R can be explained as follows. Above the P–R transition point  $T_{tr}$ , the clusters are mainly oriented along the  $z$ -axis according to the persistence of the QES in the (ZZ) spectra. This feature is in agreement with the results reported in [1], which show that the displacement of Nb ions is along the [001] direction in the R phase. The behaviour of the QES integrated intensity with temperature reflects the dynamics of these clusters which are clearly linked to the mechanism of the phase transitions, as revealed by the critical change of the  $J(\text{QES})$  intensity in the vicinity  $T_{tr}$  (figure 6(a)). On approaching  $T_{tr}$  from below, the rapid increase of the QES and the soft-mode integrated intensities, as well as the dielectric permittivity [10], show that the correlations between relaxing dipoles and the cluster size increase. Such phenomena were previously observed for FE compounds such as  $\text{KNbO}_3$  [11] and KTN [12].

#### 5. Summary

In this work we have studied the phase transition from the P phase to the R phase in sodium niobate crystal by means of Raman scattering measurements. We have for the first time revealed the occurrence of an anisotropic QES besides the LFM in both P and R phases of the crystal, reflecting the presence of dynamic polarized clusters in the AFE state. The phase transition from P to R in  $\text{NaNbO}_3$  crystal can be described in terms of a mechanism induced by relaxing dipoles around off-centre Nb ions, reflecting an order–disorder character of the AFE phase transition.

## References

- [1] Lefkowski I, Lukazewicz K and Megaw H D 1966 *Acta Crystallogr.* **20** 670
- [2] Glazer A M and Megaw H D 1973 *Acta Crystallogr. A* **29** 489
- [3] Darlington C N W and Knight K S 1999 *Physica B* **266** 368
- [4] Wang X B, Shen Z X, Hu Z P, Qin L, Tang S H and Kuok M H 1996 *J. Mol. Struct.* **385** 1
- [5] Molak A, Paweczyk M and Kwapulinski J K 1994 *J. Phys.: Condens. Matter* **6** 6833
- [6] Chen J and Feng D 1988 *Phys. Status Solidi a* **109** 171
- [7] Konieczny K 1999 *Mater. Sci. Eng. B* **60** 124
- [8] Cross L E and Nicholson B J 1955 *Phil. Mag.* **46** 453
- [9] Shen Z X, Wang X B, Kuok M H and Tang S H 1998 *J. Raman Spectrosc.* **57** 379
- [10] Konieczny K and Kajtoch Cz 1998 *Ferroelectrics* **215** 65
- [11] Fontana M D, Ridah A, Kugel G E and Carabatos-Nedelec C 1988 *J. Phys. C: Solid State Phys.* **21** 5853
- [12] Bouziane E and Fontana M D 1997 *J. Phys.: Condens. Matter* **9** 10249
- [13] Ridah A, Fontana M D and Bourson P 1997 *Phys. Rev. B* **56** 5967
- [14] Roleder K, Maglione M, Fontana M D and Dec J 1996 *J. Phys.: Condens. Matter* **8** 10669
- [15] Kania A, Roleder K, Kugel G E and Fontana M D 1986 *J. Phys. C: Solid State Phys.* **19** 9